Towards a Real-Time Automated Eco-driving Algorithm Based on Human Cognition with Drivability Constraints

Edwin Solano-Araque, Guillaume Colin, Guy-Michel Cloarec, Abdel-Djalil Ourabah, Yann Chamaillard

Towards a Real-Time Automated Eco-driving Algorithm Based on Human Cognition with Drivability Constraints

Edwin Solano-Araque, Guillaume Colin, Guy-Michel Cloarec, Abdel-Djalil Ourabah, Yann Chamaillard

***Abstract*—Driving automation offers a great potential for reducing environmental impact of road transports. Automated eco-driving, i.e. adapting vehicle behaviour in order to reduce energy consumption is a way of achieving it. However, for an eco-driving algorithm to be implemented in a commercial vehicle some constraints on drivability, safety and computing power are to be addressed. In this paper, we propose an acceleration maneuver model allowing to explicitly consider drivability constraints. The model is based on many empirical studies on Physiology and Ergonomics and has been verified using real driving recordings. Then we propose an Automated Eco-driving algorithm, allowing to minimize driving energy consumption while meeting drivability and safety constraints. The algorithm is able to adapt to changes in the driving scenario and its architecture is compatible with a real-time implementation.**

***Index Terms*—Eco-driving, Real-time Control, Automated Driving, Connected and Autonomous Vehicles, Optimal Control, Electric Vehicles.**

I. Introduction

REDUCING the environmental impact of road transport has become a priority. In this context, Connected and Autonomous Vehicles (CAV) offer significant potential for lowering vehicles' in-use energy consumption and could play a key role in the transition towards sustainable mobility [1], [2]. These vehicles are equipped with environmental sensors that provide valuable information about driving conditions, which can be used to reduce energy consumption. One way to achieve this is by adapting vehicle's dynamic behavior (or *driving style*) in order to improve overall efficiency, commonly referred to as **Eco-driving** [3], [4], [5]. This also has the potential to extend the range of Electric Vehicles (EV), a major concern for this type of vehicles [6], [7], [8].

For Eco-driving algorithms to be widely implemented on commercial vehicles, several important constraints must be respected: these must be safe, able to adapt to changes in the driving scenario and must guarantee comfort which gives the drivability constraints. The review of the state of the art [9], summarized at the beginning of the article, provides clear physiologically justified criteria for enforcing drivability. These criteria align with empirical observations in the field of human ergonomics and are presented in a way that simplifies their consideration for control algorithms. Based on these theories of human physiology, drivability constraints can be defined as limits on maximal and minimal accelerations, on maximal and minimal jerks (derivative of acceleration) and on maximal and minimal acceleration durations. To achieve this, one can draw inspiration from human cognitive mechanisms. Furthermore, it is also important for Eco-driving algorithms to be compatible with real-time operation and efficient enough to run on embedded systems.

In the literature, several solutions have been proposed to address the problem of eco-driving [10]. Eco-driving can be written as an Optimal Control Problem (OCP) [4], [11], where system's states are speed and position. This complete OCP problem can be solved by Dynamic Programing (DP) [1]. The main characteristics of DP solution are an off-line global optimum depending on the mesh, but as expressed in [12], its computational complexity becomes a limiting factor. To mitigate computational challenges, a receding-horizon OCP can be solved using the Model Predictive Control (MPC) framework as in [13], [14], [15], [16], [17] or with bi-level optimization [18].

To further reduce computational demands, real-time eco-driving algorithms have been proposed based on the Pontryagin Minimum Principle as in [19], [20], [21]. Some drivability constraints could also be incorporated such as [3], [22], [23], [24]. For example, in [1], an explicit acceleration limit is considered for an analytical solution of the Eco-driving OCP for EV's. A real-time approach to implement it is presented in [25]. Most of these approaches aim to solve the eco-driving problem by finding the optimal vehicle speed trajectory [10]. However, they often overlook human behavior and driver perception when addressing safety and drivability constraints, particularly with regard to jerk [26]. Moreover, an important factor for an industrial implementation of Eco-driving algorithms is the capacity to adapt to changes in the driving scenario. This is crucial as input data generally comes from prediction of future conditions. While few works consider this aspect, [21], [25] present offer some approaches to address it.

To tackle these challenges and explicitly take into account safety and drivability constraints, this paper proposes an approach that finds the optimal acceleration and jerk by dividing trips into individual maneuvers. Moreover, the current algorithm proposes a new approach for adapting to changes in the driving scenario that explicitly takes into account drivability and safety considerations. Hence, our proposed algorithm will

G. Colin and Y. Chamaillard are with PRISME Laboratory, Univ. Orléans, INSA, France, e-mail: guillaume.colin@univ-orleans.fr.

A.-D. Ourabah and G.-M. Cloarec are with Renault S.A.S., France

E. Solano-Araque was with Renault S.A.S and PRISME lab, France, email: esolano77@unab.edu.co

Manuscript received November 15, 2024

have several advantages: respect human ergonomy, mimic human behavior, consider drivability and safety constraints by design, minimize energy consumption, be real-time capable and ease the tuning.

Hence, the main contributions of this paper can be summarized as follows:

- the generation of the drivability constraints based on physiology and driving ergonomics state of the art,
- a human cognition friendly maneuver model validated on real driving experiments,
- an off-line optimisation to determine energy optimal maneuvers set points,
- a real time capable Eco-driving algorithm based on trapezoidal maneuvers that adapts to changes in the driving conditions,
- a comparison of the proposed algorithm to a classical state of the art result (Intelligent Driving Model, IDM [27]) and to real maneuvers.

Note that the present work is the subject of patents [28], [29].

This paper is then organized as follows. Section II describes how a human could be mathematically modeled from ergonomy literature and empirical observations. A complete elementary maneuver model that respect human ergonomy is then deduced and validated on real driving data. From that, in section III, an energy management algorithm which applies optimal driving maneuvers is proposed. Afterwards in section IV, results from testing and tuning this algorithm on a simulation of an EV are discussed and compared to the IDM and real driving. Finally, section V includes some conclusions and perspectives for future work.

II. Ergonomics Modeling of a Driving Maneuver

Drivability is a major issue in designing CAV. For an Automated Driving System (ADS) to be adopted by the user, it not only needs to take into account safety and energy consumption performances; vehicle behavior should fit well with what a driver would expect and appreciate.

In order to better understand what makes a vehicle behavior to be pleasant (or to be unpleasant) one should consider the way the human body perceives movement. Therefore, in this section we will present some results on Physiology and Driving Ergonomics, that will be the basis for proposing an ergonomic model of a driving maneuver. For a more detailed presentation of this review and of our own conclusions and hypothesis, the reader is invited to consult [9].

A. General Vestibular Function Principle

In addition to visual and acoustic cues, the human body is capable of perceiving its movement by means of what is called the Vestibular Function (VF) [30]. The VF allows an individual to perceive his own movement as well as the gravitational field acting on him. It is mainly (yet not uniquely) related to the Vestibular System (VS), located in the internal ear [31], [32], [33]. The VS consists of two main subsystems [34]: the **Semicircular Canals** (horizontal, posterior and anterior), related to rotational movement and orientation perception, and the **Otholitic Organs (OO)** (utricle and saccule), related to linear movements.

OO play a main role in drivability perception as they are related with translational movement. This is especially true for the utricle, the organ responsible for movement perception in the horizontal plane [34], [35], [36], [37], [38]. Each OO is made up of an patch of sensory and support cells called *macula*, covered with a gelatinous membrane, the *otolithic membrane*, which contains on its top calcium carbonate crystals, known as *otoliths* or *otoconial crystals*. Embedded in the otolithic membrane are clusters of hairs coming from the *Vestibular sensory cells* in the macula's support layer, the *Neuro-epithelial Layer*. There are two kinds of cell hairs: a unique hair at the extreme of the cell, the *kinocilium*, and all the other hairs, called *Stereocilia*. This is represented by Fig. 1.

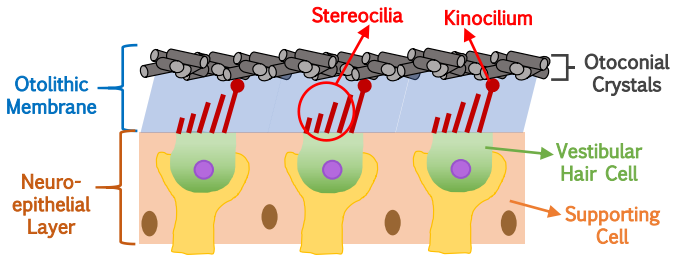

Fig. 1. Otolithic Organs anatomy (based on [34], [35], [36], [39], [37], [38])

When the head moves linearly, the inertia of the otoliths make them resists to the movement, bending the gelatinous layer and the hairs within. It generates a polarisation or depolarisation in the hair cells that will be communicated to the brain [34], [40].

One implication of this mechanism is that constant speed movement is not perceived by the VS as its response depends on inertial effects. Another implication is that, when the head is bowed, gravitational effects will act on the VS and generate a response affecting translationnal movement perception. Applied to driving, this means that **speed *variation* will have a main impact on drivability perception** and **road slope will affect the sensitivity of the driver to the vehicle behavior**. This is schematized in Fig. 2 for a longitudinal dynamics with slope.

Curthoys et al. propose the existence of two kinds of VS, associated with two different zones of each vestibular organ: the Sustained Vestibular System (SVS) and the Transient Vestibular System (TVS) [42]. The former is responsible of perceiving steady vestibular stimuli, as constant and low frequency accelerations and head tilt. The latter is in charge of sensing transient stimuli, high frequency accelerations and jerk (acceleration's derivative). Therefore, **a driver is sensible to both acceleration and jerk, respectively related to steady and transient vehicle speed variations**.

As it has been pointed out, the utricle is the OO responsible for movement perception on the horizontal plane. As lateral and longitudinal translations are sensed by the same organ, it comes that **lateral behavior of a vehicle will affect the**

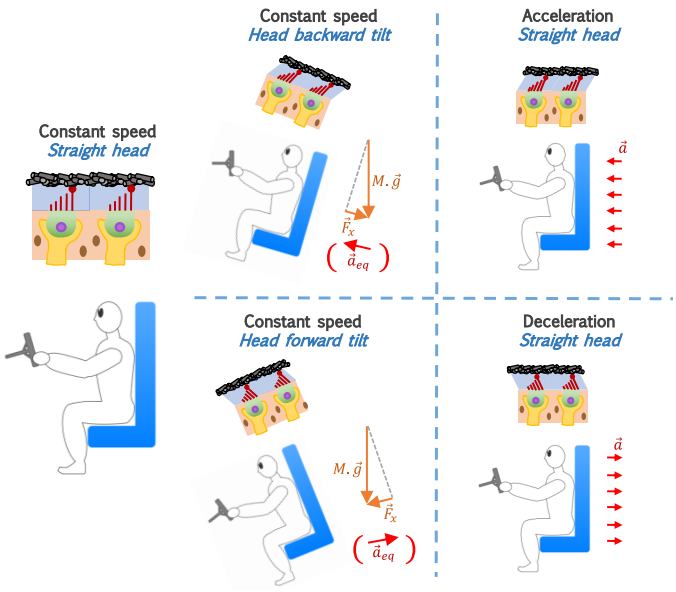

Fig. 2. General Vestibular movement perception in a longitudinal vehicle (based on [34], [41]). Seat inclination and head tilt are not represented here

drivability perception of the longitudinal behavior. It means that drivability constraints will depend on the road curvature.

By looking at the way the sensory cells are distributed on the utricle, one can conclude that, depending on whether the individual undergoes an acceleration or a deceleration, different cells will be inhibited and activated [35], [38], [43], [44]. **It might result in a difference in the way a driver perceives vehicle acceleration and deceleration**.

Finally, *in vivo* studies in mammals tests show that the neural response to constant acceleration and jerk stimuli vary depending on the duration of the input [45], [46]. This means that **there might be an influence of the topology of the vehicle acceleration profile and the drivers comfort**. Hence, in order to rightly evaluate comfort, evaluating acceleration and jerk instantaneous values is not enough; one should also consider the duration and sequence of steady and transient acceleration phases.

B. Empiric Observations in Ergonomics Studies

So far, we have considered the physiological mechanisms influencing driving comfort perception, particularly looking at results from animal *in vivo* and *in vitro* experiments. We will now consider studies on humans, either using *ad hoc* vehicles or platforms or driving experience on simulation or on the road. For sake of conciseness, We will limit our presentation to some main results with direct implications for drivability.

In [47] (as cited by [48]), different acceleration profiles were applied on a panel of passengers standing on a small car moving on a smooth track. The drivability criterion considered was the "loss of balance" associated to the passenger either grabbing a handrail or moving either foot. Subjects experienced a greater difficulty to keep balance when acceleration varied very quickly than when it increased linearly with a constant jerk. Also, higher jerk values led to a higher loss of balance than lower jerk values.

In [49] passengers on a modified trolley were subjected to symmetric trapezoidal acceleration profiles and their capacity to maintain stability was studied. It was found that comfort does not depend only on acceleration values but also in jerk levels. It was also shown that stronger jerk levels can be accepted provided that the acceleration at the top the trapezium is kept low.

Both studies suggest that **jerk levels and overall topology of the acceleration profile have a great influence on drivability**.

Muller et al studied the minimum variation in jerk and acceleration values than a driver can perceive [50], called *just noticeable difference*. They applied stimuli to participants in a modified vehicle. For considered acceleration variations, constant jerk was applied; for studying jerk effect on drivers, the same end acceleration was used. **The tests showed that there is a threshold of variation of acceleration and jerk that the driver cannot perceive**. It may be useful for the design of ADS. The just noticeable differences determined were $0.1[m/s^2]$ for acceleration and $1[m/s^3]$ for jerk.

In a study conducted on real vehicles in urban/rural and highway environments, Bellem et al looked for objective metrics allowing to differentiate between three driving styles [51]. A remarkable contribution of theirs is **considering drivability through a maneuver-based analysis**. They showed that **some maneuver-specific metrics such as acceleration, jerk, quickness (the inverse of the maneuver duration) and headway distance (in seconds) allow to differentiate between driving styles**. Hence, these features are likely to have a strong influence on drivability. The difference between the metrics relevant for urban and highway settings highlights that **driving context plays an important role on driving comfort perception**. Also, in this research, **maneuvers are represented as sequences of basic actions**. We will exploit this idea when proposing a maneuver model.

Ikonen et al performed a study on experienced drivers in a simulation platform [52]. The goal was to investigate relationships between jerk, acceleration and time headway in a controlled environment. They found strong correlations between jerk and acceleration values and also an inverse relation between time headway and jerk values. These results indicate that **time headway has an important influence on driver behavior and on his perception of comfort**. An ADS should therefore guarantee to maintain an acceptable distance with the preceeding vehicle.

In Bellem et al a moving-base simulation platform is used to study drivers preference on acceleration and jerk in lane changes, acceleration and deceleration scenarios [53]. For the acceleration and deceleration scenarios, different types of acceleration profiles were considered, showing a difference in drivers comfort perception. In particular, **symmetrical acceleration profiles seem to improve drivability assessement**. This shows that **maneuver topology plays an important role on driving comfort**.

C. Mathematical Formalization of a Driving Maneuver Model

Starting from the results presented below, we will now propose a vehicle dynamics model taking into account ergonomic

considerations. As we have seen, drivability seems to be better assessed when considered on a maneuver basis. Therefore, we will propose an acceleration maneuver model.

First, we need to define a maneuver: *A driving maneuver is the vehicle trajectory allowing it to pass from a "quasi-steady" state, from the driver's perspective, to another "quasi-steady" state*. A *quasi-steady* state is the situation where the driver gets a minimal (relative) vestibular stimulus and where he has no action to perform other than keeping the vehicle controls in the current position. This corresponds to driving on a straight line while keeping a roughly constant speed. Some examples of maneuvers covered by this definition are: acceleration after a speed limit change, turning, line-changing, deceleration behind a preceding vehicle, maintaining speed during a strong slope variation, etc. However, the scope of this work will be longitudinal maneuvers.

The modeling principle we propose consists in representing a maneuver as an acceleration profile constituted by a sequence of transient (Fig. 3b) and steady acceleration phases (Fig. 3a). This coheres with the physiological response of a human driver: during transient phases the TVS will be active, as the SVS will be so during steady acceleration phases. Here, we will only consider *elementary maneuvers*, i.e., those in which the acceleration level only gets close to 0 $[m/s^2]$ at the beginning and the end of the profile; more complex or *compound maneuvers* can be produced by the concatenation of elementary maneuvers, but it is out of the scope of this paper.

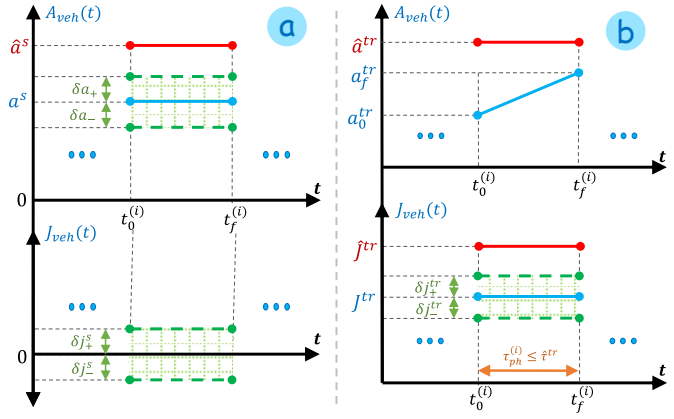

Fig. 3. Model of Steady and Transient phases of an acceleration maneuver. a) Steady phases, b) Transient phases.

1) Steady-acceleration phases: correspond to the time intervals within a maneuver where the acceleration is subjected to weak fluctuations. In these phases, acceleration has the most influence in comfort due the SVS behavior. Acceleration during steady phases a^s is supposed almost constant, i.e. inside an acceptable range, corresponding to the just noticeable acceleration difference for a driver, and defined by the tolerance values δa_- and δa_+ as shown in Fig. 3a. Likewise, jerk should be kept within the driver's perception threshold, defined by δj^s_- and δj^s_+. In order to guarantee driving comfort, the steady-phase acceleration should not exceed a drivability threshold $\hat{a}^s$.

2) Transient-acceleration phases: In these phases, jerk has the greatest influence on driving comfort due to the TVS. We will consider here that jerk remains at a roughly constant level, J^{tr}, during transient phases, as shown in Fig. 3b. Drivability requires jerk to be kept below a threshold $\hat{J}^{tr}$. Acceleration should also remain under a certain limit, $\hat{a}^{tr}$, but these condition will usually be covered by the drivability constraint of steady phases. As in the case steady phases, jerk should not exceed a tolerance range defined by δj^{tr}_- and δj^{tr}_+.

TVS response seems to be dependent on stimulus duration, as shown by empirical test at Renault S.A.S. and in [54], [46]. Therefore, we should introduce a constraint in the transient phase duration, $\tau_{ph} \leq \hat{\tau}^{tr}$, where $\hat{\tau}^{tr}$ is the maximal duration for the jerk limit J^{tr}. $J^{tr} = f(\hat{\tau}^{tr})$ can be identified on empirical driving data [9].

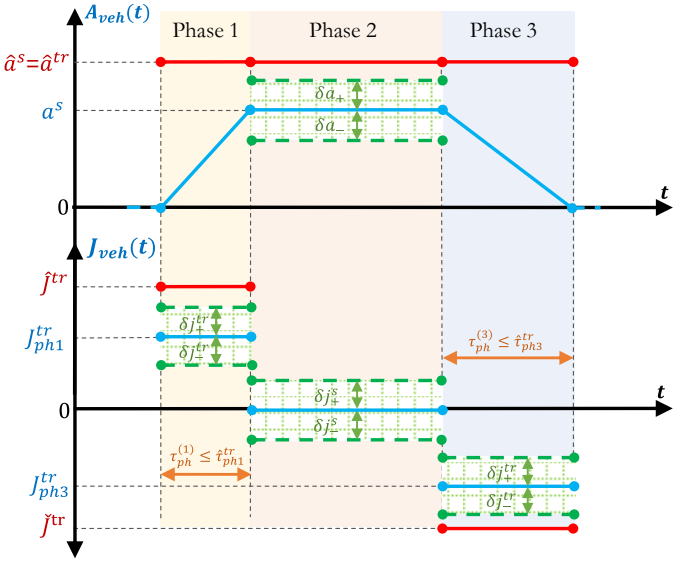

Fig. 4. Complete acceleration maneuver model.

3) Complete elementary maneuver model: By combining, transient and steady phases, it is possible to propose different maneuver topologies, e.g. the *trapezoidal acceleration maneuver*, Fig. 4. At the beginning, the vehicle moves at constant (possibly 0 $[m/s]$) speed, then during **Phase 1** vehicle acceleration increases (or decreases) at a constant rate J^{tr}_{ph1}; next, in **Phase 2** acceleration is kept constant at a^s for some time until one gets close to the desired speed; then, **Phase 3** starts and acceleration decreases at a constant jerk J^{tr}_{ph3} until reaching the final speed. From now on, vehicle speed will remain constant until the next maneuver.

Real driving recording have been performed in an instrumented car riding between Guyancourt and Versailles (France). The total recording duration was 3470s and it was made during two different days. By using these recordings, we were able to check that the trapezoidal topology represents well the vehicle behaviour in some driving scenarios. This is shown in Fig. 5, were trapezoidal profiles were identified from the recordings. The value denoted as p_r is the Pearson coefficient which was used to assess the quality of the identification [55]. One can see that the model fits well the data. The signal treatment applied to the recorded signal is presented in [56].

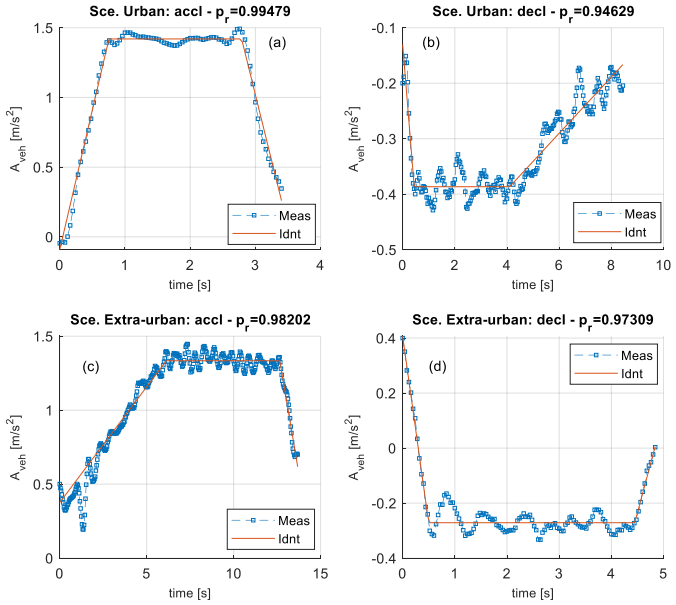

Fig. 5. Validation of the trapezoidal acceleration model of maneuvers with real driving data.

As we will see in the next section, the proposed model can be used for the design of longitudinal dynamics control function. Its use for guaranteeing drivability while controlling some of the vehicle's actuators can be done [29].

III. Algorithm for Applying Optimal Longitudinal Driving Maneuvers

In this section we will focus on how to exploit our analysis and modeling of driving ergonomics for the design of efficient ADS. For this, we propose an algorithm architecture inspired by some features of human cognition related to skill acquisition and problem-solving, compatible with real-time implementation. The proposed algorithm is the subject of the patent [28].

A. Algorithm's Architecture

The algorithm we propose is inspired by principles of human cognition associated with skill learning and problem-solving, as presented in chapter 9 of [57]. It is composed of 4 interacting subsystems (Fig. 6):

- **Constraints generation** allows to define constraints, based on information from the vehicle's internal and environmental sensors, safety and drivability, compatible with the driving context.
- **Energy optimization** solves the optimization problem and allows to find the optimal maneuver for the current driving scenario, taking into account safety and drivability constraints.
- **Kinematics Control of the Vehicle** manages the timing of the different maneuver phases, based on the optimal driving maneuver, while adapting the acceleration profil to changes in the driving scenario. It produces an instantaneous acceleration setpoint.
- **Actuators Setpoint Definition** generates a torque (or force) setpoint for the powertrain, allowing to reach the desired acceleration value.

We will present below how the formulation and working principle of the last three subsystems, as well as some simulation results. The safety and drivability constraints are supposed to be known; we have used some values based on the analysis of empirical data as the one shown in Fig. 5. The considered scenario was taken from a real driving situation, recorded at the route D91 leading to Versailles, France; the scenario consists in the instrumented vehicle slowing down before a truck in a three-way road with slightly dense traffic conditions.

B. Off-line Energy Optimization of Driving Maneuvers

1) Optimization Problem Formulation: As shown in section II, a trapezoidal acceleration profile (Fig. 4) will allow to produce a right vehicle behaviour that the driver will found familiar enough. The acceleration profile is given by (1), where $a_{ph1}(t) = a_0 + J_1 t$, $a_{ph2}(t) = a_{ex}$, $a_{ph3}(t) = J_3\left[\frac{a_{ex}-a_0}{J_1} + \tau_2 + \frac{a_{ex}}{J_3}\right] - J_3 t$, $\tau_1 = \frac{a_{ex}-a_0}{J_1}$ and $\tau_3 = \frac{a_{ex}}{J_3}$. An acceleration maneuver will therefore be defined by the value of the parameter vector $\underline{\theta} = [a_{ex}, J_1, J_3, \tau_2]^T$.

$$A_{veh}(\underline{\theta},\, t) = \begin{cases} a_{ph1}(\underline{\theta},\, t) & , \quad 0 \le t < \tau_1 \\ a_{ph2}(\underline{\theta},\, t) & , \quad \tau_1 \le t < \tau_1 + \tau_2 \\ a_{ph3}(\underline{\theta},\, t) & , \quad \tau_1 + \tau_2 \le t \le \tau_1 + \tau_2 + \tau_3 \end{cases} \tag{1}$$

The optimal trapezoidal maneuver from time 0 to t_f, that respects all the safety and drivability constraints, can be found off-line by solving the optimization problem (2) in order to find the high-level parameters $\underline{\theta}$ of this driving maneuver.

$$\underset{\underline{\theta} \in \mathbb{R}^r}{\text{minimize}} \quad E_{mnv}(\underline{\theta}) = \int_0^{t_f(\underline{\theta})} P_{bat}(\underline{\theta},\, t)\, dt \tag{2a}$$

$$\text{subject to} \quad V_f^h = V_{veh}(t_f) = V_0^h + \frac{{a_{ex}}^2 - {a_0}^2}{2\,J_1} + a_{ex}\tau_2 + \frac{{a_{ex}}^2}{2\,J_3} \tag{2b}$$

$$\Delta\check{X}_{mnv} \le \Delta X_f(\underline{\theta}) \le \Delta\hat{X}_{mnv} \tag{2c}$$

$$\check{\tau}_{mnv} \le t_f(\underline{\theta}) \le \hat{\tau}_{mnv} \tag{2d}$$

$$\tau_1(\underline{\theta}), \tau_2(\underline{\theta}), \tau_3(\underline{\theta}) \ge 0 \tag{2e}$$

$$\check{a}_{mnv} \le a_{ex} \le \hat{a}_{mnv} \tag{2f}$$

$$\check{J}_{mnv} \le J_1 \le \hat{J}_{mnv} \tag{2g}$$

$$\check{J}_{mnv} \le J_3 \le \hat{J}_{mnv} \tag{2h}$$

The instantaneous power consumption $P_{bat}(\underline{\theta},\, t)$, as a function of time t and of the maneuver parameters $\underline{\theta}$, can be found by applying the acceleration profile defined in (1) to a vehicle consumption model. The numerical and analytical consumption models $P_{bat}(\underline{\theta},\, t)$ could be found in [5], [9].

The equality constraint (2b) imposes that the host vehicle (or *ego-vehicle*), whose initial speed is V_0^h, should attain the desired speed V_f^h at the end of the maneuver. It is a safety condition. In the case of speed limit changes, V_f^h will be equal to the next allowed maximal speed; in the case of a deceleration maneuver allowing to reach the vehicle ahead, we will have $V_f^h = V_f^t$, where V_f^t will be a prediction of the *target* vehicle speed at the end of the maneuver.

Equation (2c) requires the gap ΔX_f between the host vehicle and its target at the end of the maneuver to be

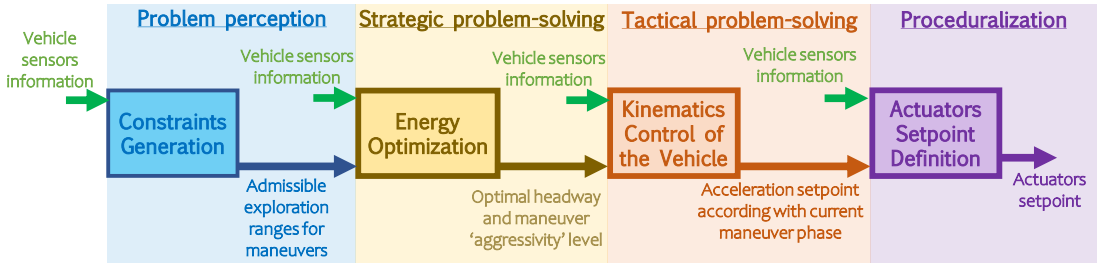

Fig. 6. Optimal maneuver algorithm structure. Each stage is associated with human cognition features, as presented in [57]

contained within a certain *acceptable corridor* as in [16], defined by the high and low limits, $\Delta\check{X}_{mnv}$ and $\Delta\hat{X}_{mnv}$, respectively. The target may be a static one (e.g., a stop sign), or a moving one (e.g., the preceding vehicle), and $\Delta X_f\,(\underline{\theta})$ definition should be adapted accordingly. When the target is another vehicle, ending too close to it may affect the safety of the host vehicle's driver and passengers; on the contrary, if the host vehicle ends too far from its target, other vehicles may overtake it and it may be bothering for the driver. In this case, ΔX_f can be deduced directly from (1):

$$\Delta X_f = \Delta X_0 + \Delta V_0\left[\tau_2 + \left(\frac{1}{J_1}+\frac{1}{J_3}\right)a_{ex}\right] - \frac{a_{ex}}{2}\left(\tau_2+\frac{a_{ex}}{J_3}\right)^2 - \frac{{a_{ex}}^3}{6}\left(\frac{1}{{J_1}^2}-\frac{1}{{J_3}^2}\right) - \frac{{a_{ex}}^2}{2\,J_1}\left(\tau_2+\frac{a_{ex}}{J_3}\right) \tag{3}$$

Box constraint (2d) for final time t_f is used to prevent the maneuver from being too *quick* $\check{\tau}_{mnv}$ (on *longitudinal quickness*, see [51]) or from taking too long $\hat{\tau}_{mnv}$. This conditions are aimed to enforce drivability. Also, causality constraints (2e) impose each of the trapezoidal maneuver phases duration to be non-negative.

Finally, constraints (2f)-(2h) allow to guarantee that vehicle's behaviour will respect drivability requirements. Box constraint (2f) is associated with driver's SVS as it is associated to vehicles acceleration a_{ex} during trapezium steady phase, i.e. between minimal $\check{a}_{mnv}$ and maximal $\hat{a}_{mnv}$ accelerations. Box constraints (2g) and (2h) are related to the driver's TVS and impose jerk during transient phases to have acceptable levels, i.e. between minimal $\check{J}_{mnv}$ and maximal $\hat{J}_{mnv}$ jerks.

For our study, the different constraint parameters are based either on empirical data analysis or on Renault S.A.S. expertise [9].

2) Optimisation Problem Solving: To solve the off-line optimisation problem (2), a brute-force algorithm is used. Some feasibility constraints should be checked. Firstly, the domain defined by (2f)-(2h) was discretized. Then, for each combination of a_{ex}, J_1 and J_3, τ_2 is deduced from (2b), and if $\tau_2 < 0$ then the maneuver is considered as non-feasible. Next, position constraint (2c) and time constraint (2d) were checked. The maneuver was considered only if it complied with all of these constraints. Finally, the optimal maneuver was determined by finding the parameters $a^\star_{ex}$, $J^\star_1$ and $J^\star_3$ minimizing energy consumption among the feasible maneuvers.

To fairly compare the different maneuvers, a correction term should be applied to the cost function. Indeed, different trapezoidal profiles will led to different travelled distances. Hence, we can define a *reference distance* that should be reached whatever the acceleration profile is. A steady speed phase is then added at the end of each trapezoidal acceleration profile so that that reference travelled distance is reached. The *corrected consumption* will be the sum of the energy expended during the maneuver and the one expended during the steady phase.

3) Optimisation Problem Results: Fig. 7 presents the corrected energy consumption as a function of the maneuver parameters and the optimal point (represented by a star). Two cases have been solved. First, an *Asymmetric Maneuver Optimization Problem* is considered, where the jerk at the beginning J_1 and at the end J_3 are independent (Fig. 7a).

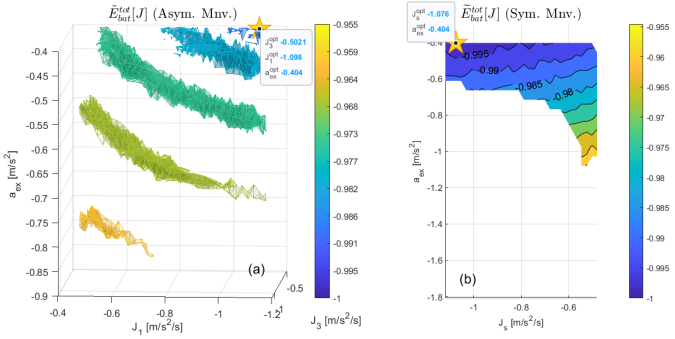

Fig. 7. Optimization results on the studied scenario. a) Asymmetric maneuver optimization problem; b) Symmetric maneuver optimization problem. Energy consumption is presented in normalized units.

The second case is *Symmetric Maneuver Optimization Problem* where the trapezoidal profile is symmetrical: $J_1 = J_3 = J_s$. The rational for studying this special case is that, as shown in [53], drivers seem to prefer symmetrical acceleration profiles and also as it allows to reduce the complexity of the optimization problem and of the Kinematic Control of the vehicle. The results of the optimization problem for the considered scenario are presented in Fig. 7b.

C. On-line Kinematic Control of Driving Maneuvers

A trapezoidal acceleration maneuver is constituted by four phases, as shown in Fig. 8a. They are the same whether we consider an acceleration or a deceleration scenario. We have:

- **Phase 0:** State of the vehicle previous to the start of the maneuver. During this phase acceleration is zero and the vehicle keeps a steady speed.

- **Phase 1:** initial transient of the maneuver. The acceleration increases at a (relatively) constant jerk until a certain acceleration is reached.
- **Phase 2:** during this phase acceleration is kept close to a constant value.
- **Phase 3:** final transient of the maneuver. Acceleration is decreased at a (relatively) constant jerk until reaching 0. At the end of this phase, the vehicle will start a new *Phase 0* and maintain at steady speed.

It is possible to generate such a profile by means of a state-machine, as shown at Fig. 8b. Each state corresponds to a phase of the trapezoidal maneuver, and the behavior of the acceleration can be easily represented by linear recursive equations. The behavior of the state machine can be described as: at *Phase 0* acceleration is zero until the flag b_{mnv} became true, indicating the beginning of *Phase 1*; during this phase, vehicle acceleration will linearly increase at each iteration until reaching a value close enough to a_{ex}; then, *Phase 2* will start and acceleration will be equal to a_{ex} until the condition associated to flag b_{ph2} is activated; at this moment, *Phase 3* begins, and acceleration will linearly decrease at each time step. Once A_{veh} gets close enough to zero, the maneuver ends and a new *Phase 0* could begin.

In order to adapt to changes in the driving scenario, at each phase our algorithm allows to change certain parameters of the trapezoidal profile. Evolution in the driving scenario will affect many kinematic parameters, such as the desired final speed, $V_h^f[k]$ and the initial headway, $\Delta X^0[k] = X_t^0 - X_h^0$. Also, the natural progress in the maneuver execution will affect the current relative speed $\Delta V^0[k] = V_t^0 - V_h^0$ and the current acceleration $a_0[k]$. Index k allows us to consider the "initial values" (i.e. the current values) of the algorithm at iteration k. The desired variation in host vehicle speed, $\Delta V^h = V_h^f - V_h^0$, and the desired headway at the end of the maneuver, ΔX_f, will be considered as the "Maneuver goals", as they will influence drivers assessment on whether a maneuver responded well to a given driving scenario.

At each iteration on **Phase 1**, jerk value J_1 will be kept constant. However, at this stage, it is still possible to change the other maneuver parameters (a_{ex}, τ_2 and J_3) without the driver realizing it. Our approach consists in modifying these parameters during this phase in order to adapt vehicle's maneuver behavior to changes in the scenario. This is done by combining constraints 2b (on final speed) and 2c (on final relative position) while fixing jerk values to the results of the optimal problem: $J_1 = J_1^\star$ and $J_3 = J_3^\star$. From (2b), we obtain:

$$\tau_2 = \alpha_1[k]\,\frac{1}{a_{ex}} + \alpha_2\,a_{ex} \tag{4}$$

where $\alpha_1[k] = \left[\Delta V^h[k] - \frac{(a_0[k])^2}{2\,J_1^\star}\right]$ and $\alpha_2 = -\frac{1}{2}\left(\frac{J_1^\star + J_3^\star}{J_1^\star\,J_3^\star}\right)$.

a_{ex} can be updated by finding the zeros of (5):

$$f(a_{ex}) = \delta_0 + \delta_1\,a_{ex} + \delta_2\,{a_{ex}}^2 + \delta_4\,{a_{ex}}^4 \tag{5}$$

where:

$$\delta_0[k] = \left[\Delta V^h[k] + \frac{(a_0[k])^2}{2J_1^\star}\right]\left(\Delta V_0[k] - \frac{\Delta V^h[k]}{2} + \frac{(a_0[k])^2}{4J_1^\star}\right) \tag{6}$$

$$\delta_1[k] = \Delta X_0[k] - \Delta X_f^\star - \frac{a_0[k]}{J_1^\star}\left[\left(\Delta V_0[k] + \frac{(a_0[k])^2}{2J_1^\star}\right) - \frac{(a_0[k])^2}{6J_1^\star}\right] \tag{7}$$

$$\delta_2[k] = \frac{1}{2}\left(\frac{1}{J_1^\star} + \frac{1}{J_3^\star}\right)\left[\Delta V_0[k] + \frac{(a_0[k])^2}{2J_1^\star}\right] - \frac{1}{2J_3^\star}\left[\Delta V^h[k] + \frac{(a_0[k])^2}{2J_1^\star}\right] \tag{8}$$

$$\delta_4 = \frac{(J_1^\star)^2 - (J_3^\star)^2}{24\,(J_1^\star)^2\,(J_3^\star)^2} \tag{9}$$

For the case of a symmetric maneuver $\delta_4 = 0$ so that $a_{ex}[k]$ is given by:

$$a_{ex}[k] = \frac{-\delta_1[k] \pm \sqrt{(\delta_1[k])^2 - 4\,\delta_2[k]\;\delta_0[k]}}{2\,\delta_2[k]} \tag{10}$$

Phase 1 ends when the condition $|A_{veh}^{sp}[k]| \geq |a_{ex}[k]|$ is met. At that moment, **Phase 2** begins and acceleration is kept constant to the value of a_{ex} when the phase shift took place ($A_{veh}^{sp}[k] = a_{ex}$). This phase will continue until the condition (11) is met, which guarantees the final speed to be close enough to the desired value V_f^h (within a tolerance defined by ε_3), as shown in Fig. 8d. Then the **Phase 3** will start. A safety condition for monitoring distance to the preceding vehicle is presented in [9].

$$b_{ph2} = \left[\left|\Delta V_0[k] - \frac{(a_{ex})^2}{2J_3^\star}\right| \leq \varepsilon_3\right] \tag{11}$$

Once car acceleration is close enough to 0, ($|a_{veh}(t)| \leq \varepsilon_0$), the current maneuver will be ended and a new **Phase 0** could start.

D. Vehicle Actuators Set-point Generation

Here, we propose a control approach allowing the application of the acceleration setpoint defined in the previous section. It is based on vehicle realistic measurements (or estimates), previous knowledge of the system and classic control techniques.

The proposed control strategy, shown in Fig. 9, allows to generate the torque signal that should be produced by the powertrain to follow the desired acceleration profile $T_{em}(t)$. This signal results from the combination of a feed-forward (or *open-loop*) term, $T_{em}^{ol}(t)$, and a closed-loop term, $T_{em}^{cl}(t)$. The value of T_{em}^{ol} can be calculated through a backward model of vehicle dynamics. In the present study, T_{em}^{cl} corresponds to a simple integral term with a Anti-Reset Windup (ARW), but more complex control strategies could be considered.

Simulation results of the control strategy are presented in the following section.

IV. Results of the Proposed Eco Driving Algorithm

A. Simulation results

Fig. 10 presents the results of applying the proposed eco-driving algorithm, under the hypothesis of perfect knowledge of the required physical quantities. The torque dynamics of the powertrain was modeled as a second-order linear system, as shown in [9]. The results are quite satisfying: the setpoint is rightly followed while keeping the jerk under an acceptable threshold. The transient behavior after t = 8s comes from

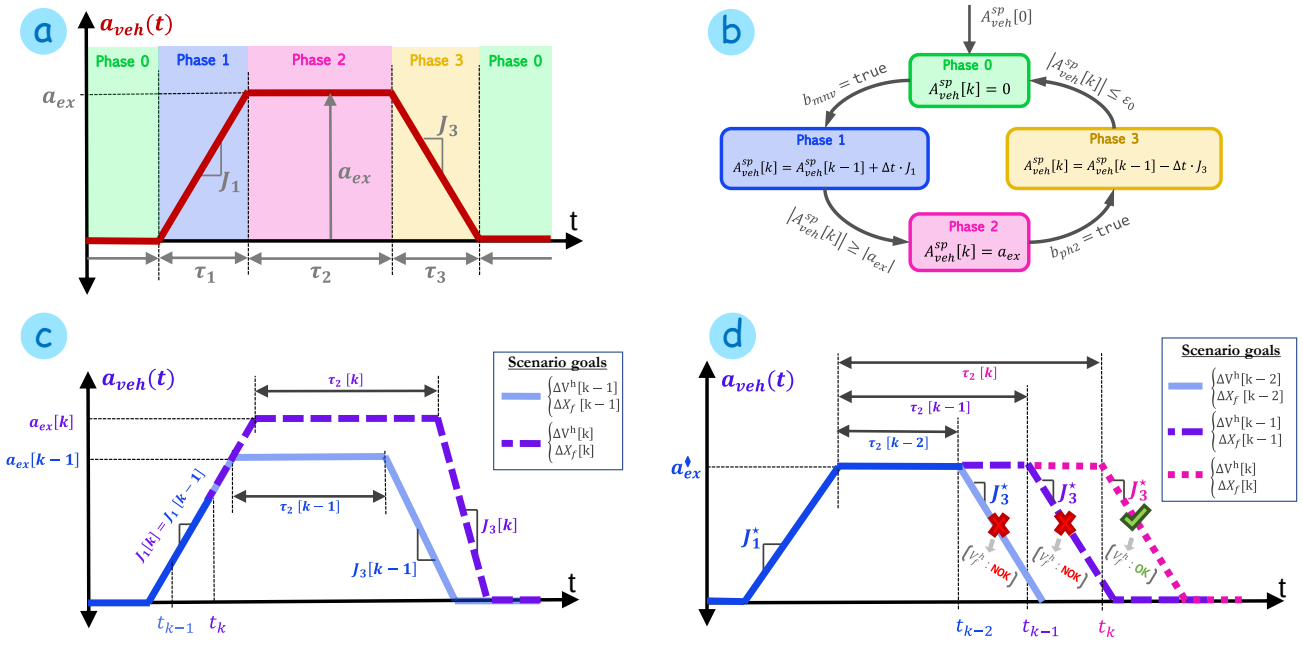

Fig. 8. Working principle of the Kinematics Control of the Vehicle. a) Maneuver phases, b) State machine algorithm's representation, c) Determination of the 1st phase duration, d) determination of the 2nd phase duration.

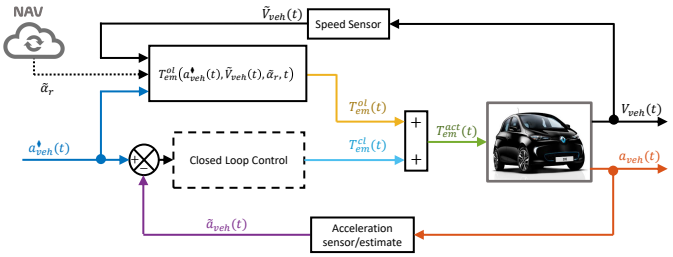

Fig. 9. Actuators setpoint generation: control structure compatible with drivability requirements.

an adaptive cruise control-like algorithm, that was activated during phase 0 at the end of the maneuver.

Fig. 10d shows actuator torque set-point, T^{ac}_{em}, as well as the effective value applied to the vehicle, T^{eff}_{em}. We notice that the main contribution to the torque value comes largely from the open-loop term, T^{ol}_{em}; nonetheless, the contribution of the closed-loop term seems to enhance the transient phases of the maneuver. Jerk threshold is slightly exceeded, but it should not affect drivability given its short duration.

B. Comparison with Intelligent Driver Model (IDM)

The algorithm is compared to the well known Intelligent Driver Model (IDM) [27], representing a realistic driving with these equations:

$$\dot{V^h}(t) = a_{max}\left(1 - \left(\frac{V^h(t)}{v_{desired}}\right)^{\delta} - \left(\frac{\Delta X^*}{\Delta X(t)}\right)^2\right) \quad (12)$$

with

$$\Delta X^* = \Delta X_0 + V^h(t)T + \frac{V^h(t)\Delta V(t)}{2\sqrt{a_{max}b_{max}}} \quad (13)$$

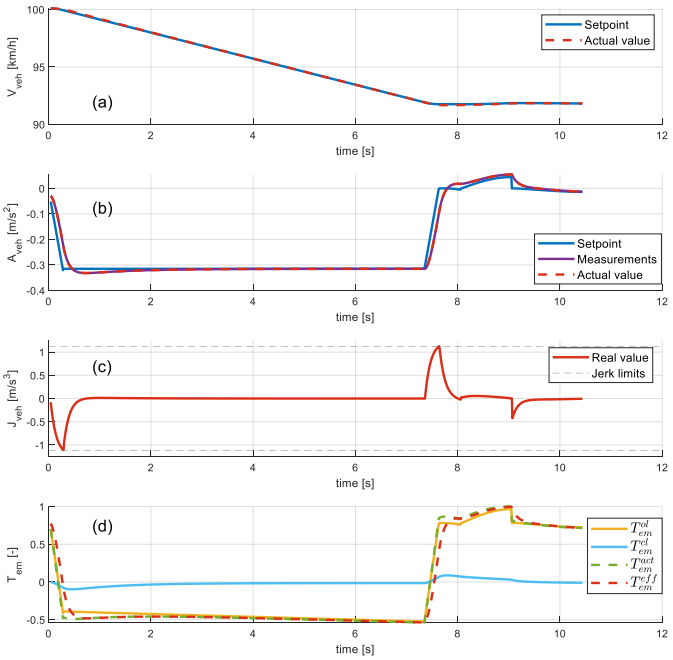

Fig. 10. Signals from the complete eco-maneuver algorithm. a) Vehicle speed; b) Acceleration; c) Jerk; d) Electric machine torque (all signals have been normalized so that the maximum value equals 1).

where V^h and ΔX are respectively host speed and distance, ΔV the velocity difference to the leading vehicle and $v_{desired}$ the desired velocity. The parameters of the IDM are: δ often chosen to 4, maximal acceleration a_{max} and braking b_{max} chosen first to 0.73 and 1.67 as in [27] and then to 0.3 as in the proposed algorithm, jam distance ΔX_0 chosen to 2m and safe time headway T. T was reduced to 1s to ensure a more precise behavior. Fig. 11 shows the results of this IDM on a

deceleration maneuver compared to the proposed algorithm. It can be noticed that the IDM jerk violates the acceptable limits ($\pm 1 m/s^3$) and the speed error is greater than 1kmph. The proposed algorithm ensure a comfortable behavior with a more precise vehicle speed.

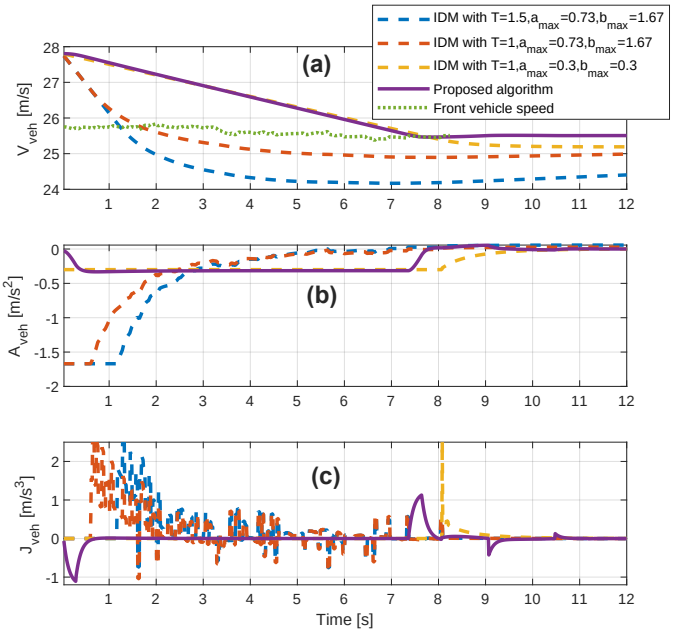

Fig. 11. Comparison of the proposed algorithm to the IDM. a) Vehicle speed; b) Acceleration; c) Jerk

C. Comparison with real driving

In Fig. 12, the performance of the proposed eco-driving algorithm is compared with an actual vehicle maneuver in a real driving situation (based on the driving recording above mentioned). Fig. 12a-12c show the kinematic signals resulting from the algorithm, as well as the signals from the actual maneuver in the real driving scenario, and the *theoretical* signals from the *Maneuver Optimization* and *Kinematic Control* stages. We verify that the final acceleration value is pretty close to the profile proposed by the *Kinematic Control* stage.

By comparing the operating points of the powertrain for the actual and the optimized maneuvers (Fig. 12d), we find that, during the non-optimal maneuver the system is constantly operating in areas of less efficiency, when compared to the optimal maneuver. In addition, in the non-optimal maneuver, the vehicle initially reaches a lower speed than desired, so the driver must accelerate and then decelerate again before reaching the target speed. So the eco-driving algorithm has reduced energy consumption by improving the system's operating points as well as avoiding compensatory accelerations and deceleration. For the studied scenario, energy consumption reduction due to the application of an optimal eco-maneuver amounts to 42.80%. Other scenarii were tested to assess the algorithm performances with effect of some delay on the acceleration signal [9].

V. Conclusions and Discussion

The work just presented is twofold. First, an approach for modeling drivability is proposed, based on the state of the art in ergonomics and various research on the vestibular system operation. Some main guidelines and hypotheses that can be applied for the design of ADS were presented. A driving maneuver model that allows to explicitly consider drivability constraints is proposed and verified based on real-driving data. This model is well-suited for the design of control algorithms.

Then, based on that model, we have proposed the functional architecture of an algorithm for optimizing driving maneuvers, to minimize energy consumption while taking into account safety and drivability constraints. The algorithm is capable of adapting to changes in the driving scenario and is compatible with real-time implementation.

The simulation results are very encouraging. And, even if the energy gain will be probably less in a real implementation of the algorithm, these results show the interest of designing ADS for the optimization of vehicle dynamics at the scale of a driving maneuver. Further studies and development of this type of system should continue, with testing and refinement in diverse environments and on different vehicles. Potential improvements to the proposed algorithm include: real-time high-level optimization of maneuver parameters (e.g., using learning-based methods or simplifying the cost function), examining the impact of jerk duration on drivability, complexifying the seat model, assessing the effects of low temperatures and slope on eco-driving performance, developing cooperative human-friendly eco-driving, and implementing the algorithm in vehicles, among others.

References

[1] A. Sciarretta and A. Vahidi, *Energy-Efficient Driving of Road Vehicles*. Springer, 2020.

[2] A. Vahidi and A. Sciarretta, "Energy saving potentials of connected and automated vehicles," *Transportation Research Part C: Emerging Technologies*, vol. 95, pp. 822–843, 2018.

[3] B. Saerens, "Optimal control based eco-driving," *Theoretical Approach and Practical Applications. Heverlee: Katholieke Universiteit Leuven*, 2012.

[4] A. Sciarretta, G. De Nunzio, and L. L. Ojeda, "Optimal ecodriving control: Energy-efficient driving of road vehicles as an optimal control problem," *IEEE Control Systems Magazine*, vol. 35, no. 5, pp. 71–90, 2015.

[5] E. Solano Araque, G. Colin, G.-M. Cloarec, A. Ketfi-Cherif, and Y. Chamaillard, "Energy analysis of eco-driving maneuvers on electric vehicles," *IFAC-PapersOnLine*, vol. 51, no. 31, pp. 195–200, 2018.

[6] M. Günther, N. Rauh, and J. F. Krems, "Conducting a study to investigate eco-driving strategies with battery electric vehicles–a multiple method approach," *Transportation Research Procedia*, vol. 25, pp. 2242–2256, 2017.

[7] M. Mruzek, I. Gajdáč, L. Kučera, and T. Gajdošík, "The possibilities of increasing the electric vehicle range," *Procedia engineering*, vol. 192, pp. 621–625, 2017.

[8] L. Thibault, G. De Nunzio, and A. Sciarretta, "A unified approach for electric vehicles range maximization via eco-routing, eco-driving, and energy consumption prediction," *IEEE Transactions on Intelligent Vehicles*, vol. 3, no. 4, pp. 463–475, 2018.

[9] E. Solano-Araque, "De l'ergonomie automobile à l'optimisation de la conduite automatisée. application à l'écoconduite de véhicules électriques," Ph.D. dissertation, Université d'Orléans - Laboratoire PRISME, 2020.

[10] J. Li, A. Fotouhi, Y. Liu, Y. Zhang, and Z. Chen, "Review on eco-driving control for connected and automated vehicles," *Renewable and Sustainable Energy Reviews*, vol. 189, p. 114025, 2024. [Online]. Available: https://www.sciencedirect.com/science/article/pii/S1364032123008833

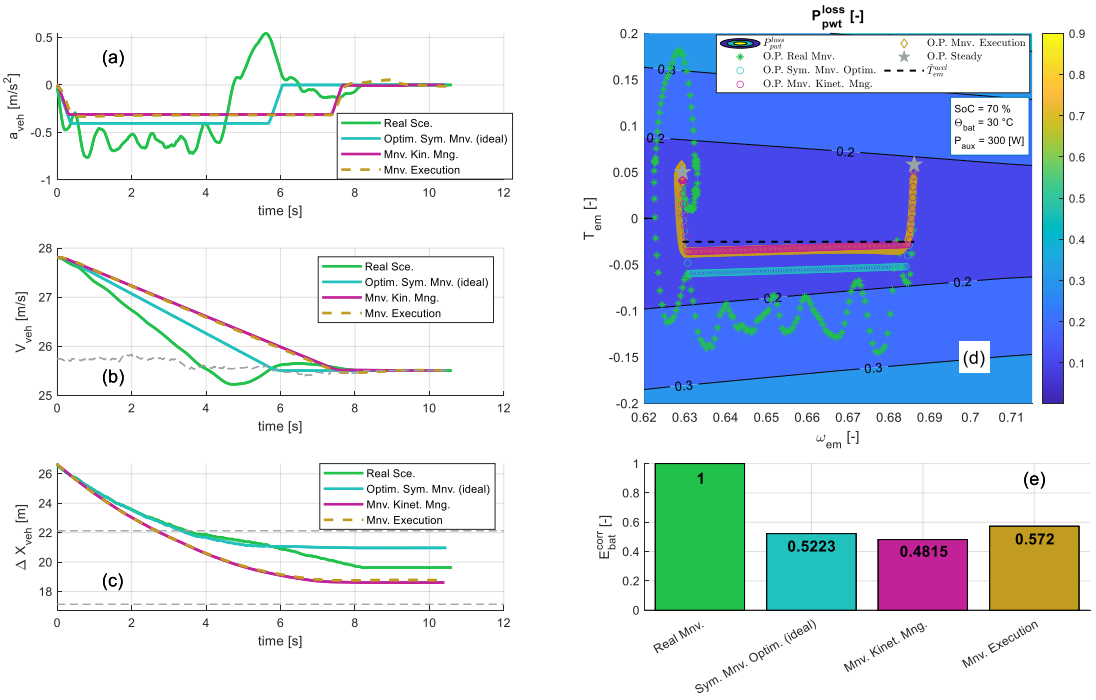

Fig. 12. Eco-maneuver algorithm results. a) Vehicle acceleration; b) Speed; c) Headway; d) Operating Points over the electric powertrain consumption map (in normalized units); e) Global normalized consumption at equivalent travelled distance.

[11] G. P. Padilla, S. Weiland, and M. C. F. Donkers, "A global optimal solution to the eco-driving problem," *IEEE Control Systems Letters*, vol. 2, no. 4, pp. 599–604, 2018.

[12] D. Maamria, K. Gillet, G. Colin, Y. Chamaillard, and C. Nouillant, "Optimal predictive eco-driving cycles for conventional, electric, and hybrid electric cars," *IEEE Transactions on Vehicular Technology*, vol. 68, no. 7, pp. 6320–6330, 2019.

[13] Y. Chen and M. Lazar, "Real-time driving mode advice for eco-driving using mpc," *IFAC-PapersOnLine*, vol. 53, no. 2, pp. 13 830–13 835, 2020, 21st IFAC World Congress.

[14] J. F. Paredes, G. P. Cazar, and M. Donkers, "A shrinking horizon approach to eco-driving for electric city buses: Implementation and experimental results," *IFAC-PapersOnLine*, vol. 52, no. 5, pp. 556–561, 2019, 9th IFAC Symposium on Advances in Automotive Control AAC 2019.

[15] N. Smit, Y. Heuts, O. Hulsebos, and M. Donkers, "Real-time optimal control for eco-driving and powertrain energy management," *IFAC-PapersOnLine*, vol. 56, no. 2, pp. 10 472–10 477, 2023, 22nd IFAC World Congress.

[16] T. Stanger and L. del Re, "A model predictive cooperative adaptive cruise control approach," in *2013 American control conference*. IEEE, 2013, pp. 1374–1379.

[17] K. Lu, Y. Chen, Y. Tong, J. Zhang, Y. Luo, and J. Wang, "Eco-driving control for cavs at signalized intersections: Adapting to traffic uncertainties," *Transportation Research Part D: Transport and Environment*, vol. 132, p. 104270, 2024.

[18] A. Hamednia, N. K. Sharma, N. Murgovski, and J. Fredriksson, "Computationally efficient algorithm for eco-driving over long look-ahead horizons," *IEEE Transactions on Intelligent Transportation Systems*, vol. 23, no. 7, pp. 6556–6570, 2022.

[19] D. Shen, D. Karbowski, and A. Rousseau, "A minimum principle-based algorithm for energy-efficient eco-driving of electric vehicles in various traffic and road conditions," *IEEE Transactions on Intelligent Vehicles*, vol. 5, no. 4, pp. 725–737, 2020.

[20] L. A. W. Ribelles, K. Gillet, G. Colin, Y. Chamaillard, A. Simon, and C. Nouillant, "Development of analytical eco-driving cycles for electric vehicles," in *2021 European Control Conference (ECC)*, 2021, pp. 1359–1366.

[21] L. L. Ojeda, J. Han, A. Sciarretta, G. De Nunzio, and L. Thibault, "A real-time eco-driving strategy for automated electric vehicles," in *2017 IEEE 56th annual conference on decision and control (CDC)*. IEEE, 2017, pp. 2768–2774.

[22] S. G. Dehkordi, M. E. Cholette, G. S. Larue, A. Rakotonirainy, and S. Glaser, "Energy efficient and safe control strategy for electric vehicles including driver preference," *IEEE Access*, vol. 9, pp. 11 109–11 122, 2021.

[23] J. Han, A. Sciarretta, L. L. Ojeda, G. De Nunzio, and L. Thibault, "Safe- and eco-driving control for connected and automated electric vehicles using analytical state-constrained optimal solution," *IEEE Transactions on Intelligent Vehicles*, vol. 3, no. 2, pp. 163–172, 2018.

[24] D. Shen, J. Han, J. Jeong, D. Karbowski, and A. Rousseau, "Receding horizon reference governor for implementable and optimal powertrain-aware eco-driving," *IFAC-PapersOnLine*, vol. 53, no. 2, pp. 13 842–13 849, 2020.

[25] C. Ngo, E. Solano-Araque, M. Aguado-Rojas, A. Sciarretta, B. Chen, and M. E. Baghdadi, "Real-time eco-driving for connected electric vehicles," *IFAC-PapersOnLine*, vol. 54, no. 10, pp. 126–131, 2021, 6th IFAC Conference on Engine Powertrain Control, Simulation and Modeling E-COSM 2021.

[26] J. Han, D. Karbowski, N. Kim, and A. Rousseau, "Human Driver Modeling Based on Analytical Optimal Solutions: Stopping Behaviors at the Intersections," *ASME Letters in Dynamic Systems and Control*, vol. 1, no. 1, p. 011010, 03 2020.

[27] M. Treiber, A. Hennecke, and D. Helbing, "Congested traffic states in empirical observations and microscopic simulations," *Physical review E*, vol. 62, no. 2, p. 1805, 2000.

[28] G.-M. Cloarec, G. Colin, O. Abdel-Djalil, and E. Solano-Araque, "Method for determining longitudinal acceleration setpoints," 2020, Patent numbers: FR20200011234,WO2021EP79792.

[29] E. Solano-Araque, G.-M. Cloarec, and G. Colin, "Method for generating a control setting for a motor vehicle component," 2022, patent numbers: FR20190008973, WO2020EP68125.

[30] C. Gianna, S. Heimbrand, and M. Gresty, "Thresholds for detection of motion direction during passive lateral whole-body acceleration in normal subjects and patients with bilateral loss of labyrinthine function," *Brain research bulletin*, vol. 40, no. 5-6, pp. 443–447, 1996.

[31] F. Hlavacka, T. Mergner, and B. Bolha, "Human self-motion perception during translatory vestibular and proprioceptive stimulation," *Neuroscience letters*, vol. 210, no. 2, pp. 83–86, 1996.

[32] H. Inagaki, T. Taguchi, E. Yasuda, and Y. Iizuka, "Evaluation of riding comfort: From the viewpoint of interaction of human body and seat for static, dynamic, long time driving," SAE Technical Paper, Tech. Rep., 2000.

[33] Y. Valko, R. F. Lewis, A. J. Priesol, and D. M. Merfeld, "Vestibular labyrinth contributions to human whole-body motion discrimination," *Journal of Neuroscience*, vol. 32, no. 39, pp. 13 537–13 542, 2012.

[34] M. E. Goldberg, M. F. Walker, and A. J. Hudspeth, "The vestibular system," in *Principles of Neural Science*, E. R. Kandel, J. H. Schwartz, T. M. Jessell, S. Siegelbaum, A. J. Hudspeth, and S. Mack, Eds. New York: McGraw-Hill Medical, 2013, ch. 40, pp. 917–934.

[35] S. Khan and R. Chang, "Anatomy of the vestibular system: a review," *NeuroRehabilitation*, vol. 32, no. 3, pp. 437–443, 2013.

[36] A. Lysakowski and J. M. Goldberg, "Morphophysiology of the vestibular periphery," in *The vestibular system*. Springer, 2004, pp. 57–152.

[37] C. J. Pastras, "Assessment of utricular nerve, hair cell and mechanical function, in vivo." Ph.D. dissertation, University of Sydney, 2018.

[38] K. Watanuki, K. Kawamoto, and S. Katagiri, "Structure of the otolithic layers on the maculae sacculi and utriculi in the guinea pig," *Equilibrium Research*, vol. 29, no. suppl-2, pp. 41–48, 1971.

[39] NeurOreille, "Otholithics organs," https://www.neuroreille.com/-levestibule/index.htm.

[40] C. Chabbert, "Anatomie et physiologie du vestibule," *EMC*, vol. 11, no. 2, pp. 1–9, 2015.

[41] D. Purves, G. J. Augustine, D. Fitzpatrick, L. Katz, A.-S. LaMantia, J. O. McNamara, and S. Williams, "Neuroscience, vol. 3," 2001.

[42] I. S. Curthoys, H. G. MacDougall, P.-P. Vidal, and C. de Waele, "Sustained and transient vestibular systems: a physiological basis for interpreting vestibular function," *Frontiers in neurology*, vol. 8, p. 117, 2017.

[43] I. S. Curthoys, V. Vulovic, L. Sokolic, J. Pogson, and A. M. Burgess, "Irregular primary otolith afferents from the guinea pig utricular and saccular maculae respond to both bone conducted vibration and to air conducted sound," *Brain research bulletin*, vol. 89, no. 1-2, pp. 16–21, 2012.

[44] M. Degironde, "Les cinétoses et leur prise en charge à l'officine," Ph.D. dissertation, Université de Toulouse III - Paul Sabatier, 2016.

[45] C. Fernandez and J. M. Goldberg, "Physiology of peripheral neurons innervating otolith organs of the squirrel monkey. i. response to static tilts and to long-duration centrifugal force," *Journal of neurophysiology*, vol. 39, no. 5, pp. 970–984, 1976.

[46] T. A. Jones, C. Lee, G. C. Gaines *et al.*, "On the high frequency transfer of mechanical stimuli from the surface of the head to the macular neuroepithelium of the mouse," *Journal of the Association for Research in Otolaryngology*, vol. 16, no. 2, pp. 189–204, 2015.

[47] C. Hirshfeld, "Disturbing effects of horizontal acceleration." Electric Railway Presidents' Conference Committee, 1932.

[48] L. L. Hoberock, "A survey of longitudinal acceleration comfort studies in ground transportation vehicles," *Journal of Dynamic Systems, Measurement, and Control*, vol. 99, no. 2, pp. 76–84, 1977.

[49] A. Browning, "Human engineering studies of high speed pedestrian conveyors," HM Stationery Office, Tech. Rep., 1972.

[50] T. Müller, H. Hajek, L. Radić-Weißenfeld, and K. Bengler, "Can you feel the difference? the just noticeable difference of longitudinal acceleration," in *Proceedings of the Human Factors and Ergonomics Society Annual Meeting*, vol. 57, no. 1. SAGE Publications Sage CA: Los Angeles, CA, 2013, pp. 1219–1223.

[51] H. Bellem, T. Schönenberg, J. F. Krems, and M. Schrauf, "Objective metrics of comfort: developing a driving style for highly automated vehicles," *Transportation research part F: traffic psychology and behaviour*, vol. 41, pp. 45–54, 2016.

[52] T. H. Itkonen, J. Pekkanen, O. Lappi, I. Kosonen, T. Luttinen, and H. Summala, "Trade-off between jerk and time headway as an indicator of driving style," *PloS one*, vol. 12, no. 10, p. e0185856, 2017.

[53] H. Bellem, B. Thiel, M. Schrauf, and J. F. Krems, "Comfort in automated driving: An analysis of preferences for different automated driving styles and their dependence on personality traits," *Transportation research part F: traffic psychology and behaviour*, vol. 55, pp. 90–100, 2018.

[54] T. A. Jones, S. M. Jones, S. Vijayakumar, A. Brugeaud, M. Bothwell, and C. Chabbert, "The adequate stimulus for mammalian linear vestibular evoked potentials (vseps)," *Hearing research*, vol. 280, no. 1-2, pp. 133–140, 2011.

[55] N. H. Bingham and J. M. Fry, *Regression: Linear models in statistics*. Springer Science & Business Media, 2010.

[56] E. Solano-Araque, G. Colin, G.-M. Cloarec, A. Ketfi-Cherif, and Y. Chamaillard, "Determining vehicle acceleration from noisy non-uniformly sampled speed data for control purposes," *IFAC-PapersOnLine*, vol. 52, no. 5, pp. 66–71, 2019.

[57] J. R. Anderson, *Cognitive psychology and its implications*. Macmillan, 2005.

Edwin Solano-Araque received an engineering degree in mechatronics from the University of Orléans (Polytech) in 2016 and from the Universidad Autonoma de Bucaramanga (Unab) in 2017. He also received a master's degree in automotive electrification and propulsion from l'Ecole Normale Supérieure de Paris-Saclay in 2016. He obtained a Ph.D. degree in energetics in 2020 from the University of Orléans, France. He spent nearly seven years studying and developing energy and pollutant reduction strategies applied to road and maritime transport for Renault Group, IFPEN, and OSE Engineering. He is currently on a leave of absence where he acts as an independent researcher while while working as an intern at Groupes Bibliques Universitaires de France. His research interests include energy management, transport, systems engineering, and automatic control.

Guillaume Colin received the master in engineering degree from École Supérieure des Sciences et Technologies de l'ingénieur de Nancy, Vandoeuvre-les-Nancy, France, in 2003, and the master's degree in automatic control. He obtained the Ph.D. degree in energetics in 2006, as well as the Habilitation to conduct research in 2013, from the University of Orléans, France. He is actually Full Professor with the University of Orléans. Since 2003, he has been with PRISME Laboratory, University of Orléans. He teaches with the School of Engineering, University of Orléans (Polytech), where he is currently the Vice-director of Polytech, in charge of education. His research interest includes powertrains and automatic control, particularly nonlinear control, and optimization.

Guy-Michel Cloarec is Research Engineer at Renault Group. He is actually Innovation Project Manager for Electric Vehicle Charge Ecosystems.

Abdel-Djalil Ourabah received an engineering degree in electronics from the University A.Mira of Bejaia, Algeria, in 2010, followed by a master's degree in intelligent systems and robotics from Pierre et Marie Curie University, Paris, France, in 2012. He then obtained his Ph.D. in computer engineering from the University of Technology of Compiegne, France, in 2018. He spent a decade at Renault Group, until mid-2023, developing new predictive and connected energy management control systems to improve the efficiency of hybrid powertrains. He now serves as Portfolio Manager for Cyber System Simulation in CATIA R&D division at Dassault. His interests span the fields of automotive, computer engineering, optimization, systems engineering and intelligent systems.

Yann Chamaillard Yann Chamaillard received the Ph.D. degree in automatic control from the University of Mulhouse, Mulhouse, France, in 1996. In 2008, he became a Full Professor with the University of Orléans, Orléans, France. He is actually Head of the INSA Centre Val de Loire. His research interests include robust and predictive control, optimization, identification, modeling for control, engine control, and energy management for hybrid vehicles.